inorganics

Review

Recent Progress in Source/Drain Ohmic Contact with β-Ga_2O_3

Lin-Qing Zhang [1], Wan-Qing Miao [1], Xiao-Li Wu [1], Jing-Yi Ding [1], Shao-Yong Qin [1], Jia-Jia Liu [1], Ya-Ting Tian [1], Zhi-Yan Wu [1,*], Yan Zhang [1], Qian Xing [2,*] and Peng-Fei Wang [3]

1 College of Electronic and Electrical Engineering, Henan Normal University, No. 46 East of Construction Road, Xinxiang 453007, China; 14110720069@fudan.edu.cn (L.-Q.Z.); lxjhjy0815@163.com (J.-J.L.)
2 College of Intelligent Engineering, Henan Institute of Technology, No. 699 Pingyuan Road (East Section), Xinxiang 453003, China
3 State Key Laboratory of ASIC and System, School of Microelectronics, Fudan University, No. 220 Han Dan Road, Shanghai 200433, China
* Correspondence: 2018010@htu.edu.cn (Z.-Y.W.); xingqian8911@163.com (Q.X.)

Abstract: β-Ga_2O_3, with excellent bandgap, breakdown field, and thermal stability properties, is considered to be one of the most promising candidates for power devices including field-effect transistors (FETs) and for other applications such as Schottky barrier diodes (SBDs) and solar-blind ultraviolet photodetectors. Ohmic contact is one of the key steps in the β-Ga_2O_3 device fabrication process for power applications. Ohmic contact techniques have been developed in recent years, and they are summarized in this review. First, the basic theory of metal–semiconductor contact is introduced. After that, the representative literature related to Ohmic contact with β-Ga_2O_3 is summarized and analyzed, including the electrical properties, interface microstructure, Ohmic contact formation mechanism, and contact reliability. In addition, the promising alternative schemes, including novel annealing techniques and Au-free contact materials, which are compatible with the CMOS process, are discussed. This review will help our theoretical understanding of Ohmic contact in β-Ga_2O_3 devices as well as the development trends of Ohmic contact schemes.

Keywords: β-Ga_2O_3; Ohmic contact; ion implantation; interface; annealing temperature

check for updates

Citation: Zhang, L.-Q.; Miao, W.-Q.; Wu, X.-L.; Ding, J.-Y.; Qin, S.-Y.; Liu, J.-J.; Tian, Y.-T.; Wu, Z.-Y.; Zhang, Y.; Xing, Q.; et al. Recent Progress in Source/Drain Ohmic Contact with β-Ga_2O_3. *Inorganics* **2023**, *11*, 397. https://doi.org/10.3390/inorganics11100397

Academic Editors: Nguyen Tuan Hung, Sake Wang and Minglei Sun

Received: 31 August 2023
Revised: 29 September 2023
Accepted: 4 October 2023
Published: 11 October 2023

1. Introduction

Si-based devices are the dominant devices used for power applications. However, with the increasing demand for much faster and more convenient network communication, Si-based device techniques cannot meet these requirements due to their physical properties. Thus, new-material devices should be investigated for operating at high temperatures, at high power, and in harsh environments. In recent years, wide-bandgap semiconductors including GaN (3.4 eV) and SiC (3.25 eV) have been developed, and they have replaced Si-based techniques in many fields due to their advantages in terms of their material properties [1–5]. Recently, β-Ga_2O_3, which is mostly thermally and chemically stable in five polymorphs [6–8], has attracted more and more attention for power applications because β-Ga_2O_3 has a wide bandgap of 4.6–4.9 eV and a breakdown field strength as high as 8 MV/cm [9–11]. In addition, for the Baliga figure and Johnson's figure of merit, when evaluating its application potential in power devices, β-Ga_2O_3 exhibits the best performance [9–11]. The basic physical properties and figures of merit (FOM) of commonly used semiconductor materials are shown in Table 1. For this reason, researchers have obtained plenty of results related to β-Ga_2O_3-based FETs [12–14], SBDs [15–18], and solar-blind ultraviolet photodetectors [19–21]. In 2023, Wang et al. [13] demonstrated a metal–heterojunction composite field-effect transistor that exhibited a breakdown voltage (BV) of around 2160 V. In addition, the corresponding $R_{ON,SP}$ was 6.35 mΩ·cm^2. So far, the power figure of merit (P-FOM) achieved the highest value of 0.73 GW/cm^2 for e-mode β-Ga_2O_3 devices. For SBDs, Hao et al. [17] used an optimized p-type NiO (with a hole concentration of 10^{17} cm^{-3}) junction-termination extension (JTE) technique that exhibited a BV and $R_{ON,SP}$ of 2.11 kV and 2.9 mΩ·cm^2, respectively. For this reason, the P-FOM was as high as 1.54 GW/cm^2. For the junction barrier Schottky (JBS) diode, Wu et al. [18] fabricated a device with a well-designed field plate to suppress the crowding effect of the electric field. The forward current and BV could reach 5.1 A and 1060 V, respectively. At the circuit level, the hybrid circuit exhibited more efficiency compared with the Si-based one. An R_{ON}-BV benchmark comparison of β-Ga_2O_3-based devices with other published results was also presented in their work. The R_{ON}-BV characteristics for β-Ga_2O_3-based devices were comparable with GaN-based ones [22]. To fully exploit β-Ga_2O_3's potential in power electronics applications, the material quality, device structure, and process details should be further optimized. By embedding indium tin oxide (ITO) electrodes, Zhang et al. [19] fabricated a fully transparent MSM-structured solar-blind UV photodetector with an excellent dark current, normalized photocurrent-to-dark-current ratio (NPDR), responsivity, rejection ratio, and specific detectivity characteristics. Another advantage of β-Ga_2O_3 material is that single large β-Ga_2O_3 crystals can be cost-effectively mass produced using melt–growth methods, such as EFG [23], FZ [24,25], VB [26,27], and CZ [28,29] methods. Additionally, a high-quality β-Ga_2O_3 epilayer can be realized using MOCVD [30,31], MBE [32,33], HVPE [34,35], and MOVPE [36,37] methods to form a well-controlled n-type doping using Si, Ge, and Sn. However, the p-type doping technique is still challenging because the activation energy of the acceptors and the self-trapping energy of the holes are large [38,39]. For the purpose of achieving p-type Ga_2O_3, great efforts have been taken by researchers from all over the world [40–51].

Table 1. Physical properties and FOMs of the commonly used semiconductors.

Parameters	Si	GaAs	4H-SiC	GaN	β-Ga_2O_3
Bandgap, E_G (eV)	1.12	1.43	3.25	3.4	4.6–4.9
Breakdown field, E_{br} (MV/cm)	0.3	0.4	2.5	3.3	8
Electron mobility, μ (cm^2 V^{-1} s^{-1})	1480	8400	1000	2000 (2DEG)	300
Saturation velocity, V_s (10^7 cm/s)	1	1.2	2	2.5	1.8–2
BFOM, $\varepsilon\mu {E_{br}}^3$	1	14.7	317	846	2000–3000
JFOM, ${E_{br}}^2{V_s}^2/(4\pi^2)$	1	1.8	278	1089	2844

For power applications, Ohmic contact is one of the key steps in β-Ga_2O_3 device fabrication processes. Ohmic contact resistance (R_C), specific contact resistance (ρ_c), and thermal stability are important indexes of contact quality. A lower R_C can reduce voltage drop across the contact region and power loss. For GaN-based devices, Au-free low-temperature Ohmic contact techniques are proposed to realize CMOS-compatible and gate-first techniques [52,53]. Until now, because of the wide-bandgap property of β-Ga_2O_3 and Fermi-level pinning [54–56], Ohmic contact methods for Ga_2O_3-based devices have remained challenging. The metal schemes, annealing conditions (the annealing temperature, durations, and atmosphere), and doping concentration of Ga_2O_3 have been investigated and optimized to obtain low-R_C contact. In this review, we will first give a brief introduction of metal–semiconductor contact theory. After that, the state-of-the-art advances in Ohmic contact techniques for β-Ga_2O_3 will be presented and discussed, including metal electrodes, surface treatments, ion implantation, epitaxial regrowth, and adding an interlayer. Finally, we will give some perspectives for further studies on Ohmic contact with β-Ga_2O_3 in the future.

2. Basic Metal–Ga_2O_3 Contact Physical Theory

Metal–semiconductor contact is a critical part of β-Ga_2O_3 power devices. A device's performance is mainly limited by the Ohmic contact property. Two types of contacts (Schottky and Ohmic) can be formed due to the differences in the work functions of contact metals [57–59]. For wide-bandgap β-Ga_2O_3, the contacts always exhibit Schottky behavior. When metal and Ga_2O_3 come into contact, the energy band of the Ga_2O_3 side bends up to make their Fermi levels equal. As shown in Figure 1a, the Schottky barrier height from the metal side (Φ_B) can be described as

$$\Phi_B = \Phi_m - \chi,$$

where χ represents the semiconductor's electron affinity (4 eV for Ga_2O_3 in our case [60]) and Φ_m represents the metal work function. Therefore, it is desirable to select a metal with a Φ_m lower than 4 eV to realize a negative Φ_B, which allows electrons to flow freely across it to form an Ohmic contact. Unfortunately, the lack of suitable metal materials with lower work functions makes Ohmic contact formation challenging. Generally, researchers have proposed Ohmic contact schemes to form a lower Φ_B or an n^+-doped Ga_2O_3 region for electron tunneling. When a semiconductor is heavily doped ($N_D > 10^{18}$ cm^{-3}), field emission (FE) dominates the electron tunneling [61,62]. In order to obtain a low R_C or ρ_c, a higher N_D is expected.

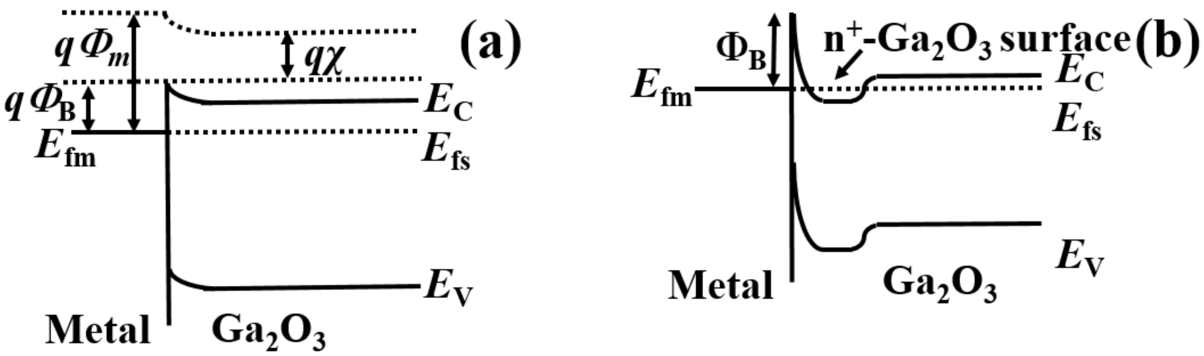

Figure 1. Energy-band diagrams of metal–Ga_2O_3 Schottky contacts with (**a**) a lower Φ_{bn} and (**b**) an n^+-doped Ga_2O_3 region.

The Ohmic contact resistance (R_C, measured in $\Omega\cdot$mm) and specific contact resistance (ρ_c, measured in $\Omega\cdot$cm^{-2}) are always determined using the transmission line model (TLM) method [63,64]. Details concerning the TLM measurement technique can be seen in the references mentioned above.

The metal work function, metal schemes, interfacial reactions between metal and a semiconductor during the annealing process, and the doping concentration of Ga_2O_3 in the source/drain region are significant influencing factors for the Ohmic contact property. Until now, researchers from universities and research institutes have proposed Ohmic contact schemes involving optimizing the metal materials, annealing condition, source/drain doping method and concentration, and source/drain etching as well as adding an interlayer in the source/drain region.

3. Approaches to Metal–Ga_2O_3 Ohmic Contact

3.1. Metal Electrode

From the metal–semiconductor contact theory, the work function of the selected metal material crucially affects the Ohmic contact quality. Thus, in the early period, Yao et al. [65] investigated the Ohmic contact properties and surface morphologies of nine metal materials, including Ti, In, Ag, Sn, W, Mo, Sc, Zn, and Zr with Sn-doped ($\bar{2}01$) β-Ga_2O_3. From their results, the work function is not the main factor influencing the contact quality. Sc, with the lowest work function, cannot form Ohmic contacts under different annealing conditions. Ti/Au metal schemes with a 400 °C annealing process exhibited the lowest R_C values. Cross-sectional transmission electron microscopy (TEM) and energy-dispersive X-ray spectroscopy (EDX) mapping showed that Ga and O diffused into the Ti layer during the annealing process. They concluded that interfacial reactions during the annealing process played a crucial part in Ohmic contact formation. Otherwise, the ultra-wide bandgap property leads to a pinning effect due to defects and surface states that lie in the mid-gap, which are not beneficial for forming an Ohmic contact.

Other groups have reported Mg/Au and Cr/Au metal schemes for Ohmic contact formation [66,67]. In the Mg (3.66 eV)/Au method, the ρ_c of 2.2×10^{-4}~2.1×10^{-5} $\Omega{\cdot}cm^{-2}$ was achieved with an annealing process at temperatures varying from 300 °C to 500 °C. Until now, the most common metallization schemes of Ohmic contact for β-Ga_2O_3 have used Ti/Au. Ti is used as an adhesion layer with a low work function. Au serves as a cap layer to prevent the oxidation of metal stacks during the high-temperature process. For the purpose of understanding the mechanism, Lee et al. [68] deposited Ti/Au (20/80 nm) on a Sn-doped β-Ga_2O_3 (010) substrate and carried out a 470 °C rapid thermal annealing (RTA) process for 1 min to form an Ohmic contact. Scanning transmission electron microscopy (STEM), high-resolution transmission electron microscopy (HRTEM), and EDX measurements were taken to understand the interfacial reactions and components. They found that a defective β-Ga_2O_3 layer (3–5 nm), a Ti–TiO_x layer (3–5 nm), and an intermixed Au–Ti layer containing Ti-rich nanocrystalline inclusions were formed sequentially, as shown in Figure 2. They deduced that the Ti–TiO_x layer (3–5 nm) with a small bandgap could provide an efficient path for the electron flow. In addition, the lattice matching between the defective β-Ga_2O_3 layer and the β-Ga_2O_3 substrate could enhance the carrier mobility by reducing the collision probability, resulting in a lower R_C. Before this work, Higashiwaki et al. [69] showed TEM results for an interface and deduced that interface reactions help improve contact quality.

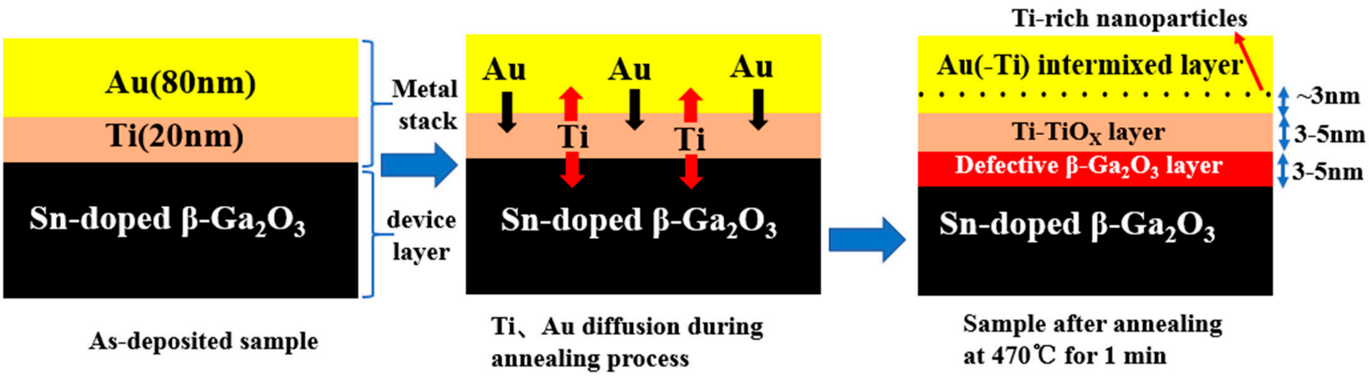

Figure 2. Schematic illustrations of Ti/Au metallization layers on Sn-doped β-Ga_2O_3 with a 1 min 470 °C N_2 annealing process. Reproduced from Ref. [68].

Also, multilayer metal contact schemes were proposed for obtaining lower R_C values, such as Ti/Al/Au [70,71], Ti/Al/Ni/Au [72,73], and Ti/Au/Ni [32,33]. As can be seen in Figure 3, Krishnamoorthy et al. formed a δ-doped β-Ga_2O_3 structure in the source/drain region to form a heavily doped contact area. After Ti/Au/Ni deposition, a 470 °C RTA process was employed for 1 min for Ohmic contact formation. The extracted R_C and ρ_c were 0.35 $\Omega{\cdot}mm$ and 4.3×10^{-6} $\Omega{\cdot}cm^{-2}$, respectively. In addition, the fabricated β-Ga_2O_3 FET exhibited excellent I_D and g_m results. By using Ti/Al/Au contact metals, Zhou et al. [71] achieved a low R_C of 0.75 $\Omega{\cdot}mm$ by adopting a highly Sn-doped channel. For AlGaN/GaN HEMT, Ti/Al/Ni/Au is one of the most mature metal schemes for Ohmic contact formation [74,75]. For β-Ga_2O_3 devices, Chen et al. [73] deposited Ti/Al/Ni/Au multilayer metal stacks and carried out an RTA process with the temperature at 470 °C for 70 s. By analyzing the X-ray photoelectron spectroscopy (XPS) results, as shown in Figure 4, they concluded that the use of Al can lead to the formation of a Ti–Al phase with a low work function, which is beneficial for oxygen vacancy generation at the interface. In n-type β-Ga_2O_3, the vacancies act as donors, enhancing the electron flow and realized Ohmic contact.

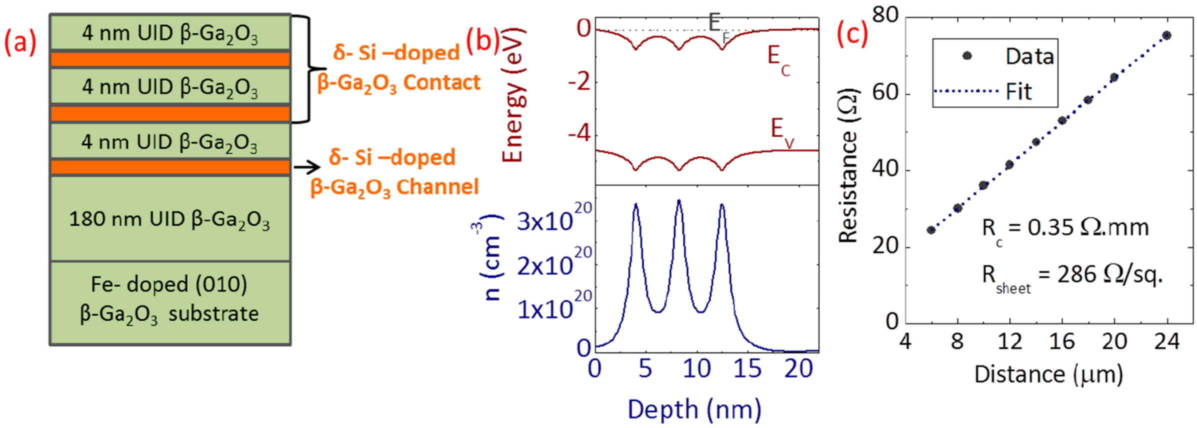

Figure 3. (**a**) Device structure, (**b**) equilibrium band diagram and charge profile, and (**c**) TLM results. Reproduced from Ref. [33].

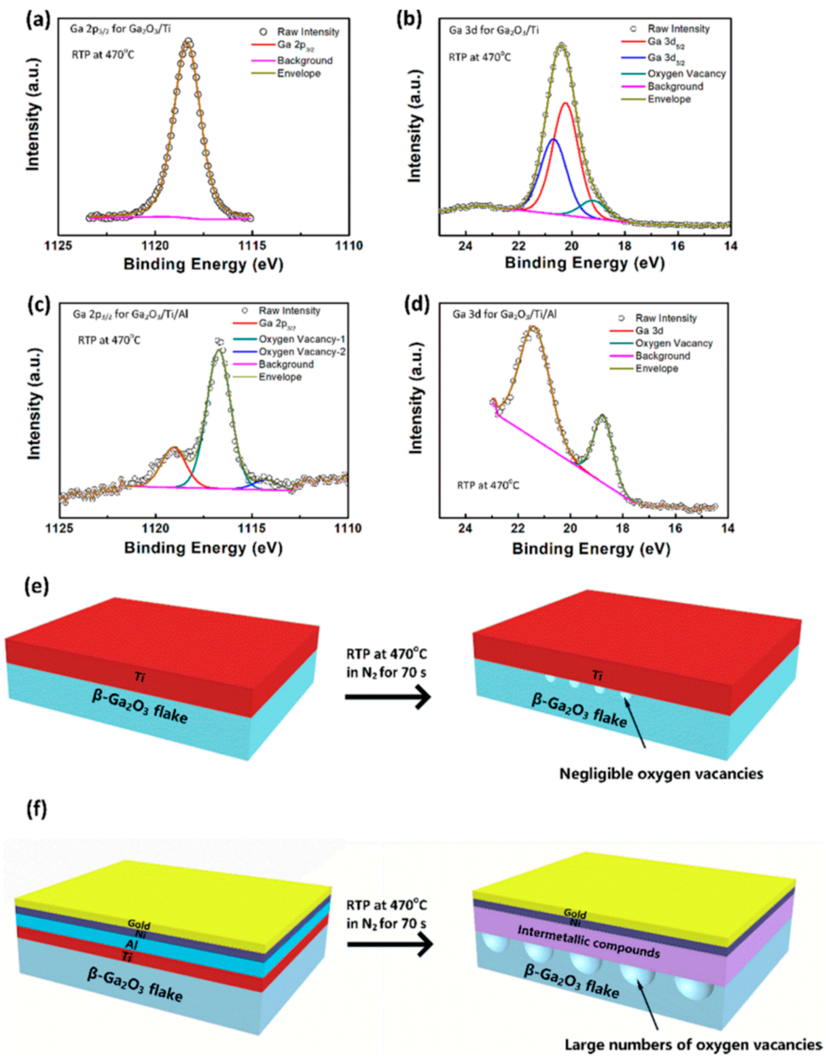

Figure 4. XPS results of (**a**) Ga $2p_{3/2}$ and (**b**) Ga 3d core-level spectra from the Ti-coated (∼2.5 nm) β-Ga_2O_3 sample. (**c**) Ga $2p_{3/2}$ and (**d**) Ga 3d core-level spectra for the Ti/Al-coated (2/2 nm) β-Ga_2O_3 sample. (**e**) Schematic diagram of the role of Ti in the generation of oxygen vacancies. (**f**) Schematic of the formation process of oxygen vacancies at the interface of β-Ga_2O_3 and metal. Reproduced from Ref. [73].

In 2022, Tetzner et al. [76] used a TiW alloy instead of the traditional Ti/Au metal schemes, and a low ρ_c of 1.5×10^{-5} $\Omega \cdot cm^{-2}$ was extracted after a 700 °C RTA process. The temperature was 200 °C higher than that of the Ti/Au schemes. To understand the Ohmic contact formation mechanism, STEM HAADF and EDX were employed. The STEM HAADF image showed that a 3–5 nm TiO_X interlayer was formed, which was confirmed with the STEM EDX. They suspected that vacancies, defects, or Ga impurities that exist in the interlayer are beneficial for electrons flowing freely to reduce the R_C.

Thermal stability is another important index of contact quality. For Ti/Au electrodes, the most commonly used annealing temperatures are between 400 °C to 500 °C. Above 500 °C, Yao et al. [65] found that the Ohmic contacts degraded in their results. In 2022, Lee et al. [77] systematically investigated the influence of temperature on Ohmic contact quality. In their results, when the annealing temperature increased from 470 °C to 520 °C, aggressive Au diffused into the interface and reacted with Ga that diffused out, resulting in a much thicker Ti–TiO_x layer due to $GaAu_2$ formation, which accounted for the contact degradation. In Kim's [78] results, the R_C increased when the temperature changed from 400 °C to 500 °C or 600 °C. They deduced that this could have been due to an increased amount of Ti oxide. Related investigations have also been conducted and reported [79–81]. Therefore, more research into interfacial reactions for Ti/Au schemes and alternative metallization schemes, including Au-free electrodes, should be proposed to solve the instability issue of the Ti/β-Ga_2O_3 interface using Ti/Au metal schemes. It should be noted that excellent Ohmic contact cannot be achieved just by selecting metal materials. Combined with other techniques, including surface treatment, ion implantation, epitaxial regrowth, adding an interlayer, etc., the contact quality can be improved and optimized.

3.2. Surface Treatment

A surface treatment before metal deposition can also help improve the Ohmic contact property (dry etching, plasma bombardment, etc.). In 2012, Higashiwaki et al. [82] compared the I–V results of Ga_2O_3 devices with and without the RIE treatment. The RIE process was implemented by using a BCl_3/Ar mixing gas for 1 min before Ti/Au (20/230 nm) deposition. The samples with the RIE treatment exhibited Ohmic contact characteristics, while without the RIE process the samples showed Schottky contact features. They speculated that the Ohmic contact formation was due to the large number of oxygen-vacancy surface defects formed during the RIE process. The defects acted as donors for Ohmic contact realization. Combined with Si ion implantation [83], they achieved a ρ_c of 4.6×10^{-6} $\Omega \cdot cm^{-2}$ with a doping concentration of 5×10^{19} cm^{-3}. In addition, Zhou et al. [70] performed an Ar plasma bombardment process and optimized the duration of 30 s for generating oxygen vacancies, which are good for n-type surface doping. The mechanism was similar to that of the BCl_3/Ar RIE process. The R_C values in their results were as low as 0.95 Ω·mm. Related results have also been reported by other groups [33,69,71,84–86].

Also, the annealing temperature and atmosphere may affect the interfacial reactions that dominate Ohmic contact formation. Bae et al. [87] compared the electrical results of the fabricated β-Ga_2O_3 nanobelts under different atmospheres with various temperatures. The samples treated under a N_2 atmosphere exhibited better characteristics that the ones treated in an air environment. Under an Ar atmosphere, Li et al. [88] reduced the R_C to 0.387 Ω·mm by optimizing the annealing temperature and the durations. In their results, a large drain current density of ~3.1 mA/μm (V_{ds} = 100 V) was achieved due to the low R_C. To fully understand the influence of an Ar atmosphere on improving the β-Ga_2O_3 device's I–V characteristics, XPS was used to show the material changes during the RTA process. From the results, as can be seen in Figure 5, they deduced that Ti reduced β-Ga_2O_3 and generated large numbers of oxygen vacancies at the interface during the annealing process, which served as effective electron donors. For this reason, the depletion layer was narrower, resulting in Ohmic behavior and a low R_C for β-Ga_2O_3 FETs. The annealing temperature is another element that affects the interface reactions to determine the Ohmic contact property. In 2022, Lee et al. [77] systematically investigated the influence of temperature (from 370 °C to 520 °C) on the Ohmic contact property. The lowest R_C occurred when temperature was 420 °C. When the temperature increased, the R_C increased as well. To investigate the reason for the degradation of the R_C with an increasing temperature, cross-sectional S/TEM was employed for a sample with an annealing temperature of 520 °C. Their results show that the thickness of the Ti-TiO_x layer (25–30 nm) increased due to the formation of $GaAu_2$ inclusions, which was caused by Au aggressively diffusing in and its reaction with Ga that had diffused out. In their early results [68], a thin Ti–TiO_x layer was beneficial for electron transport. The degradation of contact quality was the result of the increasing Ti–TiO_x layer thickness. Also, in earlier results, the degradation of contact characteristics was observed when the annealing process was performed above 500 °C [65]. Yao et al. speculated that Ti reduces Ga_2O_3, possibly forming an insulating oxide layer at the interface, which would account for the Ohmic contact degradation. In their results, the optimized annealing temperature was 400 °C, which achieved the lowest R_C value.

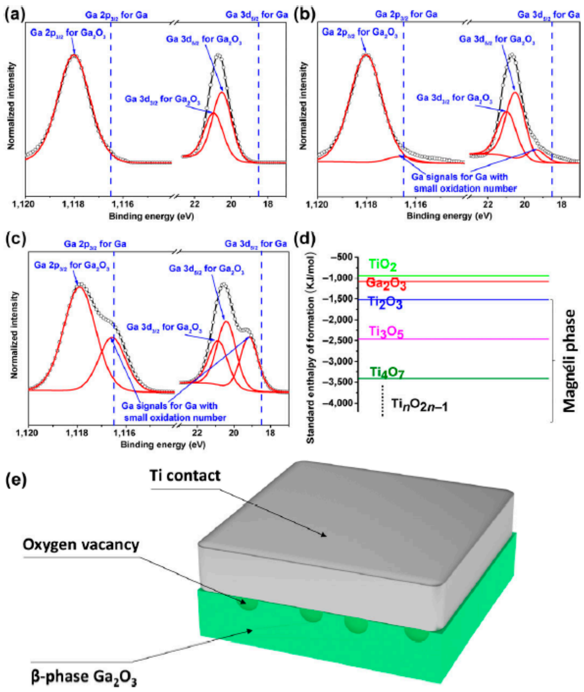

Figure 5. XPS results from β-Ga_2O_3. (**a**) Normalized Ga $2p_{3/2}$ XPS spectra and Ga 3d XPS spectra from pure β-Ga_2O_3, (**b**) β-Ga_2O_3 after annealing in argon at 300 °C for 180 min, and (**c**) Ti-coated (1 nm) β-Ga_2O_3 after annealing in argon at 300 °C for 180 min. Black dots show experimental data, and red curves show simulated fitting curves. (**d**) Free energy scheme of different metal oxides. (**e**) Schematic diagram of the proposed oxygen vacancy model at the Ti/β-Ga_2O_3 interface. Reproduced from Ref. [88].

Surface treatment, including BCl_3/Ar RIE and Ar plasma bombardment, before metal deposition can help to reduce the R_C to a degree. During these processes, the accelerated high-energy ions react with Ga_2O_3 via physical and chemical methods, creating defects to form a highly damaged surface, which enables high recombination rates. However, excellent Ohmic contact cannot be achieved only using such methods. Techniques, including RIE, ion implantation, RTA, etc., are always used together to improve the Ohmic contact quality. In addition, the RIE technique is not always reproducible or practically applicable due to the undesired damage induced during semiconductor processing.

3.3. Ion Implantation

The ion-implantation doping technique (including Si, Sn, etc.) is another effective way for Ga_2O_3 to realize low-contact-resistance Ohmic electrodes by forming a heavily doped n^+ region that facilitates electron flow. In 2013, Sasaki et al. [83] successfully fabricated Ohmic electrodes with a low contact resistance via Si implantation, which requires the MOVPE method in β-Ga_2O_3. They optimized the Si doping concentration to 5×10^{19} cm^{-3}, which was activated by annealing at a temperature of 950 °C. The R_C and ρ_c in their results were as low as 1.4 mΩ·cm and 4.6×10^{-6} $\Omega \cdot cm^{-2}$, respectively. In other results, Zhou et al. [70] doped β-Ga_2O_3 with Sn at a concentration of 2.7×10^{18} cm^{-3}. Combined with Ar plasma bombardment, the R_C was dramatically reduced to 0.95 Ω·mm. The fabricated devices also exhibited an excellent on/off ratio and output characteristics and a low SS value. In addition, Ge and Sn were also studied for doping β-Ga_2O_3 [89]. In that study, the samples were treated under the same annealing condition (925 °C for 30 min). The efficiencies of Sn, Ge, and Si were calculated to be 28.2%, 40.3%, and 64.7%, respectively, using SIMS measurements. The same activation annealing condition for Ge and Sn with Si resulted in low activation efficiencies for Ge and Sn. The heavier Ge and Sn ions also created more implant damage than the Si ions due to the greater momentum transfer required to achieve the same implant depth, likely contributing to decreased implant activation and increasing both the contact and sheet resistances. In 2023, Tetzner et al. [90] analyzed the optimized annealing temperature for the activation of Ge-implanted β-Ga_2O_3 from 900 to 1200 °C using a pulsed RTA technique. The lowest recorded ρ_c value of 4.8×10^{-7} Ω cm^{-2} was achieved after a pulsed RTA at 1100 °C using 40 pulses. The activation efficiency was 14.2%. The measured R_C and ρ_c values at various annealing temperatures can be seen in Figure 6. Also, other representative studies related to the ion implantation technique have been reported [91–94].

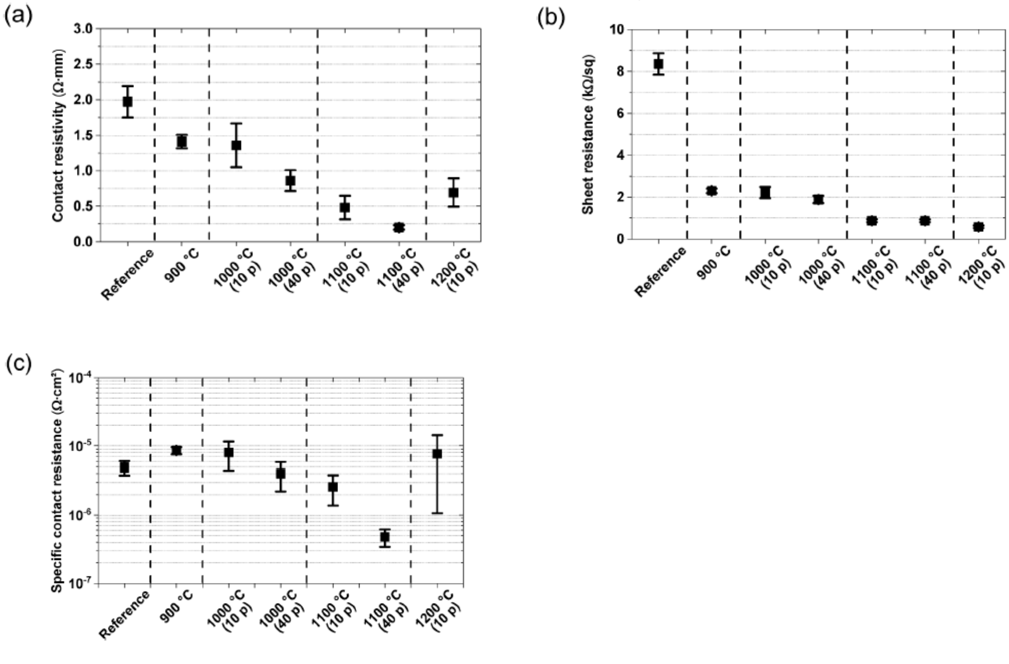

Figure 6. Measured contact resistivity (**a**), R_C (**b**), and specific contact resistance (**c**) as a function of the annealing conditions. Reproduced from Ref. [90].

Considering the high cost of ion implantation, the complicated steps, and the potential damage-induced diffusion of species, Zeng et al. [95] successfully proposed a Sn spin-on-glass (SOG) technique for β-Ga_2O_3 doping. A Sn-doped epitaxial layer with a doping density of 1×10^{18} cm^{-3} was formed on a Ga_2O_3 substrate. The obtained ρ_c was determined to be $2.1 \pm 1.4 \times 10^{-5}$ $\Omega \cdot cm^{-2}$ in their results. As shown in Figure 7, the fabricated devices also exhibited improved output current, peak transconductance, on/off ratio, and breakdown voltage values. The SOG technique is an effective alternative to the simple, low-cost doping technique to make low-R_C Ohmic contact. Thus, based on the existing results using doping techniques, it is possible to form a heavily doped Ga_2O_3 layer and obtain ρ_c values from 10^{-5} to 10^{-7} $\Omega \cdot cm^{-2}$.

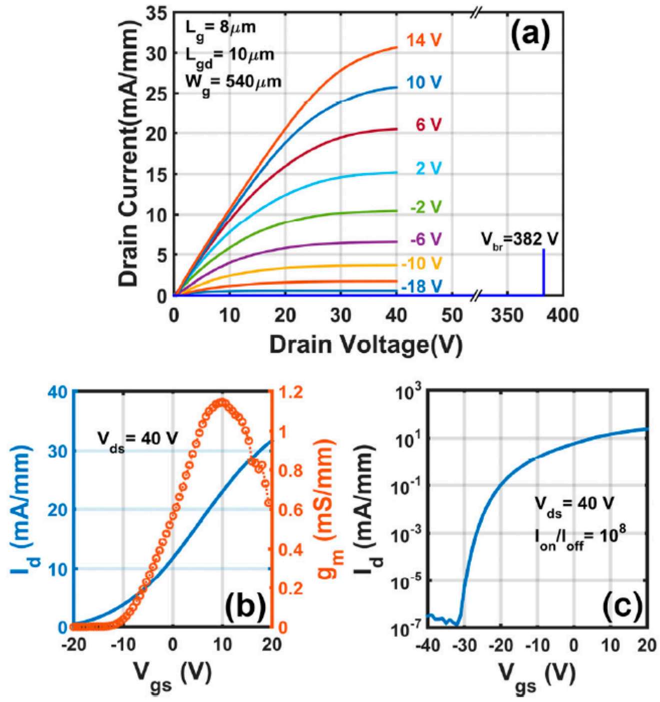

Figure 7. (**a**) Output characteristics of the SOG-doped MOSFET and (**b**,**c**) linear and log-scale transfer characteristics of the same device. Reproduced from Ref. [95].

Ion implantation, surface treatment, and post-RTA annealing are always used together to obtain a low R_C. Ion implantation can form a heavily doped interface to enhance electron tunneling. A surface treatment combined with RTA can generate oxygen vacancies that act as donors in Ga_2O_3, resulting in a low R_C. For ion implantation, a high-temperature post-anneal is required to activate the implanted donor impurity and recover the induced crystalline damage. During the high-temperature process, dopant redistribution, residuals, crystalline defects, and incomplete activation should be noticed and optimized.

3.4. Epitaxial Regrowth

To further reduce the contact resistance, regrown contacts have been reported to fabricate Ohmic contacts. Ion implantation and spin-on-glass techniques need a high annealing temperature around 900–1200 °C and potentially deteriorate the material quality in the active region. However, the regrowth process, which is performed at a much lower temperature of about 600 °C can avoid this potential problem. In 2018, Xia et al. [32] used a molecular-beam epitaxy (MBE) method to form a heavily doped n-type Ga_2O_3 with a doping concentration of 2×10^{20} cm^{-3}. The device's structure can be seen in Figure 8. An extracted R_C of 1.5 Ω·mm was obtained from the TLM structure. The regrowth technique avoids gate recessing and potential damage associated with etching, which may degrade the carrier mobility. The fabricated devices exhibited a peak drain current of 140 mA/mm and an excellent transconductance of 34 mS/mm. Considering the advantage of high room-temperature electron mobility values (close to the theoretical limit) grown using metalorganic vapor phase epitaxy (MOVPE), Bhattacharyya et al. [36] proposed an MOVPE epitaxy approach to realize low-resistance regrown S/D contacts in a Ga_2O_3 lateral MESFET for the first time. As shown in Figure 9, the heavily Si-doped (∼1.8×10^{20} cm^{-3}) Ga_2O_3 was grown using MOVPE at a relatively low temperature of 600 °C. After that, an Ohmic metal stack of Ti/Au/Ni (20 nm/100 nm/30 nm) was evaporated, followed by 470 °C annealing in N_2. From their testing results, an ultralow R_C of 80 mΩ·mm and a ρ_c of 8.3×10^{-7} Ω·cm^{-2} were achieved. In order to systematically study the mechanism of heavily doped β-Ga_2O_3 using MOVPE to achieve low contact resistance, in 2022 Alema et al. [96] optimized the doping concentration to 3.23×10^{20} cm^{-3}, and the R_C and ρ_c values were as low as 1.62×10^{-7} $\Omega \cdot cm^{-2}$ and 0.023 Ω·mm. The ultralow contact characteristics had a significant impact, improving the RF devices' performance.

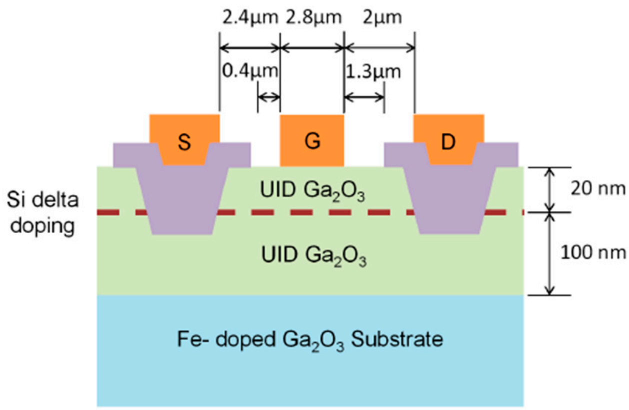

Figure 8. Device schematic of delta-doped β-Ga_2O_3 MESFET. Reproduced from Ref. [32].

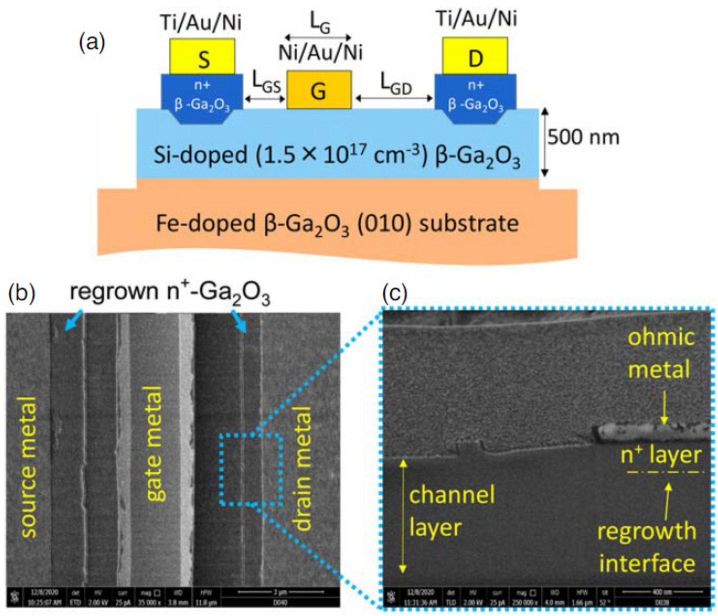

Figure 9. (**a**) Schematic of the fully MOVPE-grown Ga_2O_3 MESFET with regrown Ohmic contacts. (**b**) Top-view SEM image of the MESFET showing the regrown access regions. (**c**) Cross-sectional SEM image of the contact region showing the estimated regrowth interface. Reproduced from Ref. [36].

The existing results that have been reported in recent years demonstrate that regrown contact is an effective approach to achieve an ultralow R_C. Epitaxial regrowth obtains a high-quality crystalline film and can be versatile. However, there are also several constraints, such as low throughput, high expense, strict material compatibility, and the need for selective growth or subsequent etchings, as mentioned in Refs. [97,98].

3.5. Adding the Interlayer

The Ti/Au schemes always form a 3–5 nm interlayer, which facilitates electron transport for Ohmic contact formation. Another approach is inserting an intermediate semiconductor layer (ISL) with a low work function and a narrower bandgap. In 2016, Oshima et al. [99] proved the insertion of indium tin oxide (ITO) for forming Ohmic contact with β-Ga_2O_3. In their results, as shown in Figure 10, the ITO method exhibited Ohmic behavior at temperatures from 900 °C to 1150 °C. However, Pt/β-Ga_2O_3 maintained Schottky contact, even at the RTA temperature of 500 °C. They also confirmed the existence of an intermediate semiconductor layer (ISL) at the interface using TEM and EDS analyses.

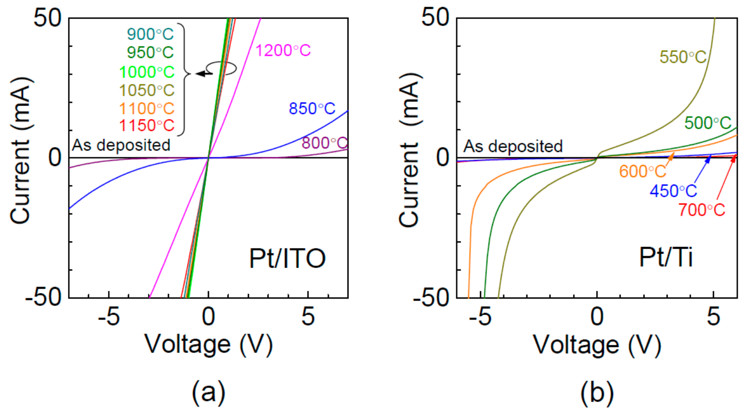

Figure 10. Typical I–V characteristics of (**a**) Pt/ITO and (**b**) Pt/Ti electrodes annealed at various temperatures. Reproduced from Ref. [99].

In 2017, considering the excellent conductivity property of ITO, by depositing an ITO layer before the metal deposition, Carey et al. created a Au/Ti/ITO/Si-doped Ga_2O_3 structure to form low-R_C contact. As shown in Figure 11, by optimizing the annealing temperature at 600 °C, the minimum R_C and ρ_c were determined to be 0.6 Ω·mm and 6.3×10^{-5} Ω·cm^{-2}. A schematic of the band offset for Au/Ti/ITO on Ga_2O_3 and Au/Ti on Ga_2O_3 can be seen in Figure 12 [100]. The insertion of an ITO interlayer allows for reduced conduction band discontinuity between Ti and Ga_2O_3, which is beneficial for reducing R_C values. By inserting an aluminum zinc oxide (AZO) interlayer [101], Au/Ti/AZO/Ga_2O_3 schemes exhibit the minimum R_C and specific contact resistance values of 0.42 Ω·mm and 2.82×10^{-5} cm^{-2}, respectively. The optimized annealing temperature is 400 °C, as shown in Figure 13. In their results, samples without an AZO interlayer did not exhibit Ohmic I–V characteristics when varying the annealing temperature. The use of a thin layer of AZO, with a bandgap of 3.2 eV, can lower the barrier for electron transport and achieve a low R_C. A corresponding schematic of the band offset for AZO on Ga_2O_3 can be seen in Figure 14. Other related results have also been presented by other researchers [102–105]. It should be noted that different metal layers capping ITO layers are needed to prevent the degradation of the surface morphology.

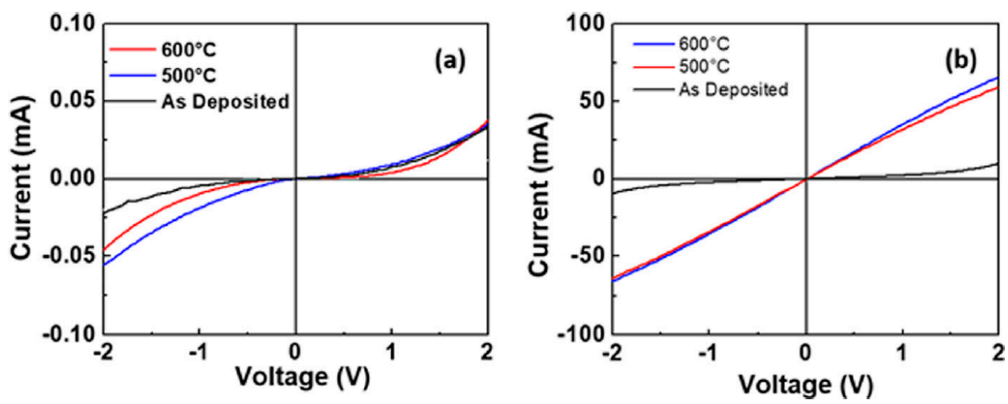

Figure 11. I–V curves of (**a**) Au/Ti/Ga_2O_3 and (**b**) Au/Ti/ITO/Ga_2O_3 contact stacks as a function of annealing temperature. Reproduced from Ref. [100].

Other elements such as substrate orientation have also been reported to influence the Ohmic contact property. To form Ohmic contact, Ti/Au contacts were deposited, followed by an RTA process at 450 °C for 5 min, which was employed on both ($\bar{2}$01) and (010) Sn-doped Ga_2O_3. The former sample exhibited Ohmic characteristics compared to the rectifying behavior of the (010) sample. Related content has also been investigated and reported by other groups [106–109].

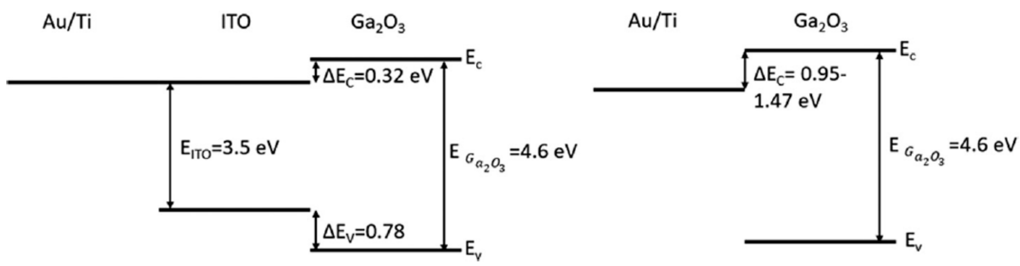

Figure 12. Schematics of band offset for Au/Ti/ITO on Ga_2O_3 and Au/Ti on Ga_2O_3. Reproduced from Ref. [100].

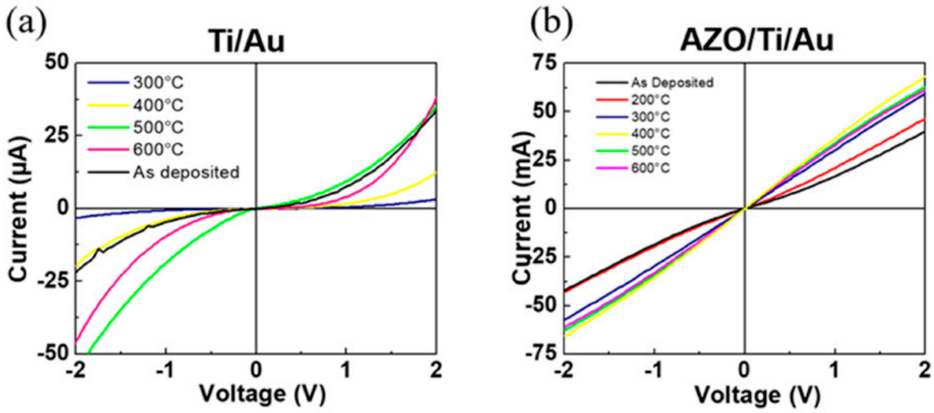

Figure 13. I–V curves of (**a**) Au/Ti/Ga_2O_3 and (**b**) Au/Ti/AZO/Ga_2O_3 contact stacks as a function of annealing temperature from as-deposited samples (black lines) to 600 °C (purple lines). The 200 °C data were similar to those of the as-deposited samples, and the contact resistance decreased with temperature in the AZO-based contacts. Reproduced from Ref. [101].

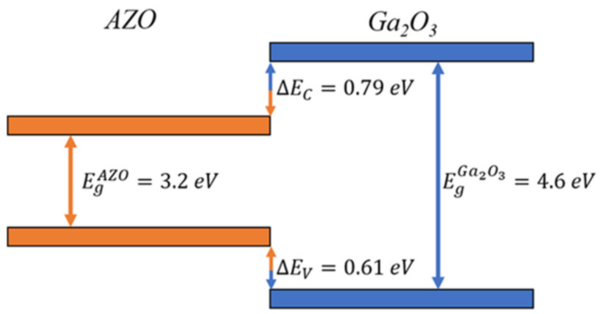

Figure 14. Schematic of band offset for AZO on Ga_2O_3. Reproduced from Ref. [101].

In recent years, researchers have investigated and optimized the Ohmic contact property of β-Ga_2O_3 by choosing a metal with a proper work function and investigating metal schemes, interfacial reactions between metal and semiconductors during the annealing process, and the doping concentration of Ga_2O_3 in the source/drain region, and they have achieved excellent results. Representative results with excellent Ohmic contact quality are summarized in Figure 15 [32,33,36,37,70,83,88,90,96,100]. Despite the significant improvement in the Ohmic contact techniques for β-Ga_2O_3, there are also some questions that need to be solved before commercializing the devices. (1) For power device applications, contact performance in high-temperature, -current, and -voltage environments is another concern. Failure analyses of the electrical stress/cycling of Ohmic electrodes have been investigated for other WBG semiconductor systems [110–112], while for β-Ga_2O_3, the research is lacking and efforts should be made to understand the degradation mechanism of Ohmic contacts under electrical stress. (2) To realize the integration of β-Ga_2O_3 semiconductors into Si CMOS technology, Au-free metal schemes should be investigated and proposed. The commonly used Ti/Au layer for Ga_2O_3 is not CMOS-compatible due to the existence of Au, which is a contaminant for Si fabrication lines [113,114]. Au is used for oxidation protection. Some oxidation-resistant capping materials, such as TiN, which has been proven to realize low-R_C Ohmic contact in AlGaN/GaN HEMT [53], can be substitutes for Ohmic contact realization in β-Ga_2O_3 devices. Related investigations should be carried out to prove the feasibility of Au-free schemes. (3) RIE, ion implantation, and epitaxial regrowth are used to achieve a low R_C. For the RIE process, the influences of plasma gas (including BCl_3/Ar, Ar, and CF_4 [115]), plasma power, bias power, etc., should be fully understood. For ion implantation, the high-temperature annealing used for impurity activation and damage recovery may cause unwanted effects, which should be noticed and further studied. In addition, the effect of substrate orientation should also be investigated. Other annealing techniques can also be used for Ohmic contact formation in β-Ga_2O_3 devices [116,117].

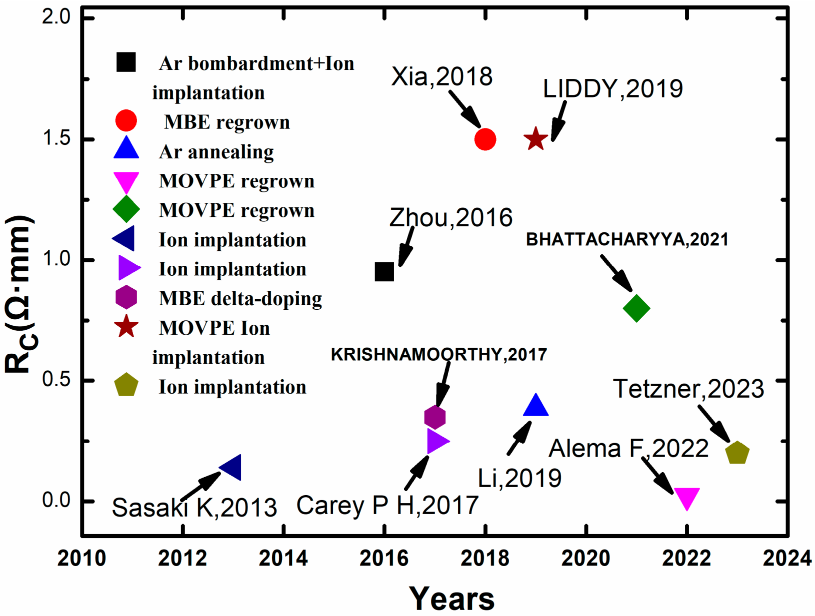

Figure 15. Research progress in source/drain Ohmic contact of β-Ga_2O_3 devices [32,33,36,37,70,83,88,90,96,100].

4. Conclusions

In this work, the β-Ga_2O_3 Ohmic contact technique has been discussed comprehensively, including the selected metal stack, surface treatment, ion implantation, epitaxial regrowth, adding the interlayer, etc. Although state-of-the-art methods for forming Ohmic contacts with β-Ga_2O_3 have been proposed and summarized in this work, there is still significant room for exploration to improve Ohmic contact, and related prospects have been proposed. In summary, Ohmic contacts with β-Ga_2O_3 will continue to be a research focus for power application in the future. We believe the content presented in this work will be beneficial for understanding and achieving high-performance β-Ga_2O_3 devices with low R_C values.

Author Contributions: L.-Q.Z.: writing—original draft, investigation, data curation, and conceptualization; W.-Q.M., X.-L.W., J.-Y.D., S.-Y.Q., J.-J.L. and Y.-T.T.: writing—original draft, investigation, data curation, and conceptualization; Z.-Y.W., Q.X., Y.Z. and P.-F.W.: writing—review and editing, visualization, and validation. All authors have read and agreed to the published version of the manuscript.

Funding: This work was supported by the Henan Province Key Research and Development and Promotion of Special Scientific and Technological Research Project (Grant No. 222102320283), key scientific research projects of higher education institutions in Henan Province (Grant No. 22B510009), and in part by the Key Laboratory of Optoelectronic Sensing Integrated Application of Hennan Province.

Data Availability Statement: The authors declare that the data supporting the findings of this study are available within the article.

Conflicts of Interest: The authors declare no conflict of interest.

References

1. Sonnenberg, T.; Verploegh, S.; Pinto, M.; Popović, Z. W-Band GaN HEMT Frequency Multipliers. *IEEE Trans. Microw. Theory Tech.* **2023**, *71*, 4327–4336. [CrossRef]
2. Akso, E.; Collins, H.; Clymore, C.; Li, W.; Guidry, M.; Romanczyk, B.; Wurm, C.; Liu, W.; Hatui, N.; Hamwey, R.; et al. First Demonstration of Four-Finger N-polar GaN HEMT Exhibiting Record 712 mW Output Power With 31.7% PAE at 94 GHz. *IEEE Microw. Wirel. Technol. Lett.* **2023**, *33*, 683–686. [CrossRef]
3. Han, L.; Tang, X.; Wang, Z.; Gong, W.; Zhai, R.; Jia, Z.; Zhang, W. Research Progress and Development Prospects of Enhanced GaN HEMTs. *Crystals* **2023**, *13*, 911. [CrossRef]
4. Li, H.; Zhao, S.; Wang, X.; Ding, L.; Mantooth, A.H. Parallel Connection of Silicon Carbide MOSFETs Challenges, Mechanism, and Solutions. *IEEE Trans. Power Electron.* **2023**, *38*, 9731–9749. [CrossRef]
5. Lyu, G.; Sun, J.; Wei, J.; Chen, K.J. Static and Dynamic Characteristics of a 1200 V/22 mΩ Normally-Off SiC/GaN Cascode Device Built with Parallel-Connected SiC JFETs Controlled by a Single GaN HEMT. *IEEE Trans. Power Electron.* **2023**, *38*, 12648–12658. [CrossRef]
6. Roy, R.; Hill, V.G.; Osborn, E.F. Polymorphism of Ga_2O_3 and the system Ga_2O_3-H_2O. *J. Am. Chem. Soc.* **1952**, *74*, 719–722. [CrossRef]
7. Yoshioka, S.; Hayashi, H.; Kuwabara, A.; Oba, F.; Matsunaga, K.; Tanaka, I. Structures and energetics of Ga_2O_3 polymorphs. *J. Phys. Condens. Matter* **2007**, *19*, 346211. [CrossRef]
8. Bechstedt, F.; Furthmüller, J. Influence of screening dynamics on excitons in Ga_2O_3 polymorphs. *Appl. Phys. Lett.* **2019**, *114*, 122101. [CrossRef]
9. Pearton, S.J.; Yang, J.; Cary, P.H.; Ren, F.; Kim, J.; Tadjer, M.J.; Mastro, M.A. A review of Ga_2O_3 materials, processing, and devices. *Appl. Phys. Rev.* **2018**, *5*, 011301. [CrossRef]
10. Wang, C.; Zhang, J.; Xu, S.; Zhang, C.; Feng, Q.; Zhang, Y.; Ning, J.; Zhao, S.; Zhou, H.; Hao, Y. Progress in state-of-the-art technologies of Ga_2O_3 devices. *J. Phys. D Appl. Phys.* **2021**, *54*, 243001. [CrossRef]
11. Sheoran, H.; Kumar, V.; Singh, R. A comprehensive review on recent developments in ohmic and Schottky contacts on Ga_2O_3 for device applications. *ACS Appl. Electron. Mater.* **2022**, *4*, 2589–2628. [CrossRef]
12. Abedi Rik, N.; Orouji, A.A.; Madadi, D. 500 V breakdown voltage in β-Ga_2O_3 laterally diffused metal-oxide-semiconductor field-effect transistor with 108 MW/cm^2 power figure of merit. *IET Circuits Devices Syst.* **2023**, *17*, 199–204. [CrossRef]
13. Wang, X.; Lu, X.; He, Y.; Liu, P.; Shao, Y.; Li, J.; Yang, Y.; Li, Y.; Hao, Y.; Ma, X. An E-mode β-Ga2O3 metal-heterojunction composite field effect transistor with a record high P-FOM of 0.73 GW/cm2. In Proceedings of the 2023 35th International Symposium on Power Semiconductor Devices and ICs (ISPSD), Hong Kong, 28 May–1 June 2023; pp. 390–393. [CrossRef]
14. Liu, H.; Wang, Y.; Lv, Y.; Han, S.; Han, T.; Dun, S.; Guo, H.; Bu, A.; Feng, Z. 10-kV Lateral β-Ga_2O_3 MESFETs with B ion Implanted Planar Isolation. *IEEE Electron. Device Lett.* **2023**, *44*, 1048–1051. [CrossRef]
15. Guo, W.; Han, Z.; Zhao, X.; Xu, G.; Long, S. Large-area β-Ga_2O_3 Schottky barrier diode and its application in DC-DC converters. *J. Semicond.* **2023**, *44*, 072805. [CrossRef]
16. Wei, Y.; Peng, X.; Jiang, Z.; Sun, T.; Wei, J.; Yang, K.; Hao, L.; Luo, X. Low Reverse Conduction Loss β-Ga_2O_3 Vertical FinFET with an Integrated Fin Diode. *IEEE Trans. Electron. Devices* **2023**, *70*, 3454–3461. [CrossRef]
17. Hao, W.; Wu, F.; Li, W.; Xu, G.; Xie, X.; Zhou, K.; Guo, W.; Zhou, X.; He, Q.; Zhao, X.; et al. Improved Vertical β-Ga_2O_3 Schottky Barrier Diodes with Conductivity-Modulated p-NiO Junction Termination Extension. *IEEE Trans. Electron. Devices* **2023**, *70*, 2129–2134. [CrossRef]
18. Wu, F.; Wang, Y.; Jian, G.; Xu, G.; Zhou, X.; Guo, W.; Du, J.; Liu, Q.; Dun, S.; Yu, Z.; et al. Superior Performance β-Ga_2O_3 Junction Barrier Schottky Diodes Implementing p-NiO Heterojuntion and Beveled Field Plate for Hybrid Cockcroft–Walton Voltage Multiplier. *IEEE Trans. Electron. Devices* **2023**, *70*, 1199–1205. [CrossRef]
19. Zhang, C.; Liu, K.; Ai, Q.; Sun, X.; Chen, X.; Yang, J.; Zhu, Y.; Cheng, Z.; Li, B.; Liu, L.; et al. High-performance fully transparent Ga_2O_3 solar-blind UV photodetector with the embedded indium-tin-oxide electrodes. *Mater. Today Phys.* **2023**, *33*, 101034. [CrossRef]
20. Li, Y.; Deng, C.; Huang, B.; Yang, S.; Xu, J.; Zhang, G.; Hu, S.; Wang, D.; Liu, B.; Ji, Z.; et al. High-Performance Solar-Blind UV Phototransistors Based on ZnO/Ga_2O_3 Heterojunction Channels. *ACS Appl. Mater. Interfaces* **2023**, *15*, 18372–18378. [CrossRef]
21. Zeng, G.; Zhang, M.R.; Chen, Y.C.; Li, X.; Chen, D.; Shi, C.; Zhao, X.; Chen, N.; Wang, T.; Zhang, W.; et al. A solar-blind photodetector with ultrahigh rectification ratio and photoresponsivity based on the $MoTe_2$/Ta: β-Ga_2O_3 pn junction. *Mater. Today Phys.* **2023**, *33*, 101042. [CrossRef]
22. Matys, M.; Kitagawa, K.; Narita, T.; Uesugi, T.; Suda, J.; Kachi, T. Mg-implanted vertical GaN junction barrier Schottky rectifiers with low on resistance, low turn-on voltage, and nearly ideal nondestructive breakdown voltage. *Appl. Phys. Lett.* **2022**, *121*, 203507. [CrossRef]

23. Aida, H.; Nishiguchi, K.; Takeda, H.; Aota, N.; Sunakawa, K.; Yaguchi, Y. Growth of β-Ga_2O_3 single crystals by the edge-defined, film fed growth method. *Jpn. J. Appl. Phys.* **2008**, *47*, 8506. [CrossRef]
24. Ohira, S.; Suzuki, N.; Arai, N.; Tanaka, M.; Sugawara, T.; Nakajima, K.; Shishido, T. Characterization of transparent and conducting Sn-doped β-Ga_2O_3 single crystal after annealing. *Thin Solid Film.* **2008**, *516*, 5763–5767. [CrossRef]
25. Víllora, E.G.; Shimamura, K.; Yoshikawa, Y.; Aoki, K.; Ichinose, N. Large-size β-Ga_2O_3 single crystals and wafers. *J. Cryst. Growth* **2004**, *270*, 420–426. [CrossRef]
26. Hoshikawa, K.; Ohba, E.; Kobayashi, T.; Yanagisawa, J.; Miyagawa, C.; Nakamura, Y. Growth of β-Ga_2O_3 single crystals using vertical Bridgman method in ambient air. *J. Cryst. Growth* **2016**, *447*, 36–41. [CrossRef]
27. Nikolaev, V.I.; Maslov, V.; Stepanov, S.I.; Pechnikov, A.I.; Krymov, V.; Nikitina, I.P.; Guzilova, L.I.; Bougrov, V.E.; Romanov, A.E. Growth and characterization of β-Ga_2O_3 crystals. *J. Cryst. Growth* **2017**, *457*, 132–136. [CrossRef]
28. Tomm, Y.; Reiche, P.; Klimm, D.; Fukuda, T. Czochralski grown Ga_2O_3 crystals. *J. Cryst. Growth* **2000**, *220*, 510–514. [CrossRef]
29. Galazka, Z.; Uecker, R.; Irmscher, K.; Albrecht, M.; Klimm, D.; Pietsch, M.; Brützam, M.; Bertram, R.; Ganschow, S.; Fornari, R. Czochralski growth and characterization of β-Ga_2O_3 single crystals. *Cryst. Res. Technol.* **2010**, *45*, 1229–1236. [CrossRef]
30. Alema, F.; Seryogin, G.; Osinsky, A.; Osinsky, A. Ge doping of β-Ga_2O_3 by MOCVD. *APL Mater.* **2021**, *9*, 091102. [CrossRef]
31. Seryogin, G.; Alema, F.; Valente, N.; Fu, H.; Steinbrunner, E.; Neal, A.; Mou, S.; Fine, A.; Osinsky, A. MOCVD growth of high purity Ga_2O_3 epitaxial films using trimethylgallium precursor. *Appl. Phys. Lett.* **2020**, *117*, 262101. [CrossRef]
32. Xia, Z.; Joishi, C.; Krishnamoorthy, S.; Bajaj, S.; Zhang, Y.; Brenner, M.; Lodha, S.; Rajan, S. Delta Doped β-Ga_2O_3 Field Effect Transistors with Regrown Ohmic Contacts. *IEEE Electron. Device Lett.* **2018**, *39*, 568–571. [CrossRef]
33. Krishnamoorthy, S.; Xia, Z.; Bajaj, S.; Brenner, M.; Rajan, S. Delta-doped β-gallium oxide field-effect transistor. *Appl. Phys. Express* **2017**, *10*, 051102. [CrossRef]
34. Oshima, Y.; Víllora, E.G.; Shimamura, K. Halide vapor phase epitaxy of twin-free α-Ga_2O_3 on sapphire (0001) substrates. *Appl. Phys. Express* **2015**, *8*, 055501. [CrossRef]
35. Murakami, H.; Nomura, K.; Goto, K.; Sasaki, K.; Kawara, K.; Thieu, Q.; Togashi, R.; Kumagai, Y.; Higashiwaki, M.; Kuramata, A.; et al. Homoepitaxial growth of β-Ga_2O_3 layers by halide vapor phase epitaxy. *Appl. Phys. Express* **2014**, *8*, 015503. [CrossRef]
36. Bhattacharyya, A.; Roy, S.; Ranga, P.; Shoemaker, D.; Song, Y.; Lundh, J.; Choi, S.; Krishnamoorthy, S. 130 mA mm^{-1} β-Ga_2O_3 metal semiconductor field effect transistor with low-temperature metalorganic vapor phase epitaxy-regrown ohmic contacts. *Appl. Phys. Express* **2021**, *14*, 076502. [CrossRef]
37. Liddy, K.J.; Green, A.; Hendricks, N.; Heller, E.; Moser, N.; Leedy, K.; Popp, A.; Lindquist, M.; Tetlak, S.; Wagner, G.; et al. Thin channel β-Ga_2O_3 MOSFETs with self-aligned refractory metal gates. *Appl. Phys. Express* **2019**, *12*, 126501. [CrossRef]
38. Varley, J.B.; Janotti, A.; Franchini, C.; Walle, C. Role of self-trap in luminescence and p-type conductivity of wide-band-gap oxides. *Phys. Rev. B* **2012**, *85*, 081109. [CrossRef]
39. Lyons, J.L. A survey of acceptor dopants for β-Ga_2O_3. *Semicond. Sci. Technol.* **2018**, *33*, 05LT02. [CrossRef]
40. Gallagher, J.C.; Koehler, A.D.; Tadjer, M.J.; Mahadik, A.; Anderson, T.; Budhathoki, S.; Law, K.; Hauser, A.; Hobart, K.; Kub, F. Demonstration of CuI as a P-N heterojunction to β-Ga_2O_3. *Appl. Phys. Express* **2019**, *12*, 104005. [CrossRef]
41. Budde, M.; Splith, D.; Mazzolini, P.; Tahraoui, A.; Feld, J.; Ramsteiner, M.; Wenckstern, H.; Grundmann, M.; Bierwage, O. SnO/β-Ga_2O_3 vertical pn heterojunction diodes. *Appl. Phys. Lett.* **2020**, *117*, 252106. [CrossRef]
42. Watahiki, T.; Yuda, Y.; Furukawa, A.; Yamamuka, M.; Takiguchi, Y.; Miyajima, S. Heterojunction p-Cu_2O/n-Ga_2O_3 diode with high breakdown voltage. *Appl. Phys. Lett.* **2017**, *111*, 222104. [CrossRef]
43. Lu, X.; Zhou, X.; Jiang, H.; Ng, K.; Chen, Z.; Pei, Y.; Lau, K.; Wang, G. 1-kV Sputtered p-NiO/n-Ga_2O_3 Heterojunction Diodes With an Ultra-Low Leakage Current Below 1μA/cm^2. *IEEE Electron. Device Lett.* **2020**, *41*, 449–452. [CrossRef]
44. Wang, Y.G.; Gong, H.H.; Lv, Y.J.; Fu, X.; Dun, S.; Han, T.; Liu, H.; Zhou, X.; Liang, S.; Zhang, R.; et al. 2.41 kV vertical P-NiO/n-Ga_2O_3 heterojunction diodes with a record Baliga's figure-of-merit of 5.18 GW/cm^2. *IEEE Trans Power Electron.* **2022**, *37*, 3743. [CrossRef]
45. Nakagomi, S.; Hiratsuka, K.; Kakuda, Y.; Yoshihiro, K. Beta-gallium oxide/SiC heterojunction diodes with high rectification ratios. *ECS J. Solid State Sci. Technol.* **2016**, *6*, Q3030. [CrossRef]
46. Zhang, Y.C.; Li, Y.F.; Wang, Z.Z.; Guo, R.; Xu, S.; Liu, C.; Zhao, S.; Zhang, J.; Hao, Y. Investigation of β-Ga_2O_3 films and β-Ga_2O_3/GaN heterostructures grown by metal organic chemical vapor deposition. *Sci. China Phys. Mech. Astron.* **2020**, *63*, 117311. [CrossRef]
47. Jaquez, M.; Specht, P.; Yu, K.M.; Walukiewicz, W.; Dubon, D. Amorphous gallium oxide sulfide: A highly mismatched alloy. *J. Appl. Phys.* **2019**, *126*, 105708. [CrossRef]
48. Cai, X.; Sabino, F.P.; Janotti, A.; Wei, S. Approach to achieving a p-type transparent conducting oxide: Doping of bismuth-alloyed Ga_2O_3 with a strongly correlated band edge state. *Phys. Rev. B* **2021**, *103*, 115205. [CrossRef]
49. Kaneko, K.; Masuda, Y.; Kan, S.; Takahashi, I.; Kato, Y.; Shinohe, T.; Fujita, S. Ultra-wide bandgap corundum-structured p-type α-(Ir, Ga) $_2O_3$ alloys for α-Ga_2O_3 electronics. *Appl. Phys. Lett.* **2021**, *118*, 102104. [CrossRef]
50. Li, Z.H.; Egbo, K.O.; Lv, X.H.; Wang, Y.; Yu, K. Electronic structure and properties of $Cu_{2-x}S$ thin films: Dependence of phase structures and free-hole concentrations. *Appl. Surf. Sci.* **2022**, *572*, 151530. [CrossRef]
51. Ezeh, C.V.; Egbo, K.O.; Musah, J.D.; Yu, K.M. Wide gap p-type NiO-Ga_2O_3 alloy via electronic band engineering. *J. Alloys Compd.* **2023**, *932*, 167275. [CrossRef]

52. Fan, M.Y.; Yang, G.Y.; Zhou, G.N.; Jiang, Y.; Li, W.; Jiang, Y.; Yu, H. Ultra-low Contact Resistivity of< 0.1 Ω mm for Au-free Ti_xAl_y Alloy Contact on Non-recessed i-AlGaN/GaN. *IEEE Electron. Device Lett.* **2020**, *41*, 143–146. [CrossRef]
53. Zhang, J.; Kang, X.; Wang, X.; Huang, S.; Chen, C.; Kei, K.; Zheng, Y.; Zhou, Q.; Chen, W.; Zhang, B.; et al. Ultralow-Contact-Resistance Au-Free Ohmic Contacts With Low Annealing Temperature on AlGaN/GaN Heterostructures. *IEEE Electron. Device Lett.* **2018**, *39*, 847–850. [CrossRef]
54. Xu, R.; Lin, N.; Jia, Z.; Liu, Y.; Wang, H.; Yu, Y.; Zhao, X. First principles study of Schottky barriers at Ga_2O_3(100)/metal interfaces. *RSC Adv.* **2020**, *10*, 14746–14752. [CrossRef] [PubMed]
55. Lovejoy, T.C.; Chen, R.; Zheng, X.; Villora, E.; Shimamura, K.; Yoshikawa, H.; Yamashita, Y.; Ueda, S.; Kobayashi, K.; Dunham, S.; et al. Band bending and surface defects in β-Ga_2O_3. *Appl. Phys. Lett.* **2012**, *100*, 181602. [CrossRef]
56. Yao, Y.; Gangireddy, R.; Kim, J.; Das, K.; Davis, R.; Porter, L. Electrical behavior of β-Ga_2O_3 Schottky diodes with different Schottky metals. *J. Vac. Sci. Technol. B* **2017**, *35*, 03D113. [CrossRef]
57. Mott, N.F. Note on the contact between a metal and an insulator or semi-conductor. In *Mathematical Proceedings of the Cambridge Philosophical Society*; Cambridge University Press: Cambridge, UK, 1938; pp. 568–572.
58. Sze, S.M.; Ng, K.K. *Physics of Semiconductor Devices*; John Wiley & Sons: Hoboken, NJ, USA, 2006.
59. Neamen, D. *Semiconductor Physics and Devices*; McGraw-Hill, Inc.: New York, NY, USA, 2002.
60. Mohamed, M.; Irmscher, K.; Janowitz, C.; Galazka, Z.; Manzke, R.; Fornari, R. Schottky barrier height of Au on the transparent semiconducting oxide β-Ga_2O_3. *Appl. Phys. Lett.* **2012**, *101*, 132106. [CrossRef]
61. Sze, S.M. *Physics of Semiconductor Devices*, 2nd ed.; Wily: New York, NY, USA, 1982.
62. Rideout, V.L. A review of the theory and technology for ohmic contacts to group III-V compound semiconductors. *Solid-State Electron.* **1975**, *18*, 541–550. [CrossRef]
63. Reeves, G.K.; Harrison, H.B. Obtaining the specific contact resistance from transmission line model measurements. *IEEE Electron. Device Lett.* **1982**, *3*, 111–113. [CrossRef]
64. Schroder, D.K. *Contact Resistance and Schottky Barriers*; Wiley: New York, NY, USA, 2006.
65. Yao, Y.; Davis, R.F.; Porter, L.M. Investigation of different metals as ohmic contacts to β-Ga_2O_3: Comparison and analysis of electrical behavior, morphology, and other physical properties. *J. Electron. Mater.* **2017**, *46*, 2053–2060. [CrossRef]
66. Shi, J.; Xia, X.; Liang, H.; Abbas, Q.; Liu, J.; Zhang, H.; Liu, Y. Low resistivity ohmic contacts on lightly doped n-type β-Ga_2O_3 using Mg/Au. *J. Mater. Sci. Mater. Electron.* **2019**, *30*, 3860–3864. [CrossRef]
67. Ma, J.; Yoo, G. Low Subthreshold Swing Double-Gate β-Ga_2O_3 Field-Effect Transistors with Polycrystalline Hafnium Oxide Dielectrics. *IEEE Electron. Device Lett.* **2019**, *40*, 1317–1320. [CrossRef]
68. Lee, M.-H.; Peterson, R.L. Interfacial reactions of titanium/gold ohmic contacts with Sn-doped β-Ga_2O_3. *APL Mater.* **2019**, *7*, 022524. [CrossRef]
69. Higashiwaki, M.; Sasaki, K.; Kamimura, T.; Wong, M.; Krishnamurthy, D.; Kuramata, A.; Masui, T.; Yamakoshi, S. Depletion-mode Ga_2O_3 metal-oxide-semiconductor field-effect transistors on β-Ga_2O_3 (010) substrates and temperature dependence of their device characteristics. *Appl. Phys. Lett.* **2013**, *103*, 123511. [CrossRef]
70. Zhou, H.; Si, M.; Alghamdi, S.; Qiu, G.; Yang, L.; Ye, P. High-Performance Depletion/Enhancement-mode β-Ga_2O_3 on Insulator (GOOI) Field-Effect Transistors with Record Drain Currents of 600/450 mA/mm. *IEEE Electron. Device Lett.* **2016**, *38*, 103–106. [CrossRef]
71. Zhou, H.; Maize, K.; Qiu, G.; Shakouri, A.; Ye, P. β-Ga_2O_3 on insulator field-effect transistors with drain currents exceeding 1.5 A/mm and their self-heating effect. *Appl. Phys. Lett.* **2017**, *111*, 092102. [CrossRef]
72. Chabak, K.D.; Moser, N.; Green, A.; Jr, D.; Tetlak, S.; Heller, E.; Crespo, A.; Fitch, R.; McCandless, J.; Leedy, K.; et al. Enhancement-mode Ga_2O_3 wrap-gate fin field-effect transistors on native (100) β-Ga_2O_3 substrate with high breakdown voltage. *Appl. Phys. Lett.* **2016**, *109*, 213501. [CrossRef]
73. Chen, J.; Li, X.; Ma, H.; Huang, W.; Ji, Z.; Xia, C.; Lu, H.; Zhang, W. Investigation of the mechanism for Ohmic contact formation in Ti/Al/Ni/Au contacts to β-Ga_2O_3 nanobelt field-effect transistors. *ACS Appl. Mater. Interfaces* **2019**, *11*, 32127–32134. [CrossRef]
74. Gong, R.; Wang, J.; Liu, S.; Dong, Z.; Yu, M.; Wen, C.; Cai, Y.; Zhang, B. Analysis of surface roughness in Ti/Al/Ni/Au ohmic contact to AlGaN/GaN high electron mobility transistors. *Appl. Phys. Lett.* **2010**, *97*, 062115. [CrossRef]
75. Fontserè, A.; Tomás, A.; Placidi, M.; Llobet, J.; Baron, N.; Chenot, S.; Cordier, Y.; Moreno, J.; Gammon, P.; Jennings, M.; et al. Micro and nano analysis of 0.2 Ω mm Ti/Al/Ni/Au ohmic contact to AlGaN/GaN. *Appl. Phys. Lett.* **2011**, *99*, 213504. [CrossRef]
76. Tetzner, K.; Schewski, R.; Popp, A.; Anooz, S.; Chou, T.; Ostermay, I.; Kirmse, H.; Würfl, J. Refractory metal-based ohmic contacts on β-Ga_2O_3 using TiW. *APL Mater.* **2022**, *10*, 071108. [CrossRef]
77. Lee, M.H.; Chou, T.S.; Bin Anooz, S.; Galazka, Z.; Popp, A.; Peterson, R. Effect of post-metallization anneal on (100) Ga_2O_3/Ti-Au ohmic contact performance and interfacial degradation. *APL Mater.* **2022**, *10*, 091105. [CrossRef]
78. Kim, Y.; Kim, M.K.; Baik, K.H.; Jang, S. Low-resistance Ti/Au ohmic contact on (001) plane Ga_2O_3 Crystal. *ECS J. Solid State Sci. Technol.* **2022**, *11*, 045003. [CrossRef]
79. Porter, L.M.; Hajzus, J.R. Perspectives from research on metal-semiconductor contacts: Examples from Ga_2O_3, SiC, (nano) diamond, and SnS. *J. Vac. Sci. Technol. A* **2020**, *38*, 031005. [CrossRef]
80. Lyle, L.A.M.; Back, T.C.; Bowers, C.T.; Green, A.; Chabak, K.; Dorsey, D.; Heller, E.; Porter, L.M. Electrical and chemical analysis of Ti/Au contacts to β-Ga_2O_3. *APL Mater.* **2021**, *9*, 061104. [CrossRef]

81. Guo, D.Y.; Wu, Z.P.; An, Y.H.; Guo, X.C.; Chu, X.L.; Sun, C.L.; Li, L.H.; Li, P.G.; Tang, W.H. Oxygen vacancy tuned Ohmic-Schottky conversion for enhanced performance in β-Ga_2O_3 solar-blind ultraviolet photodetectors. *Appl. Phys. Lett.* **2014**, *105*, 023507. [CrossRef]
82. Higashiwaki, M.; Sasaki, K.; Kuramata, A.; Masui, T.; Yamakoshi, S. Gallium oxide (Ga_2O_3) metal-semiconductor field-effect transistors on single-crystal β-Ga_2O_3 (010) substrates. *Appl. Phys. Lett.* **2012**, *100*, 013504. [CrossRef]
83. Sasaki, K.; Higashiwaki, M.; Kuramata, A.; Masui, T.; Yamakoshi, S. Si-ion implantation doping in β-Ga_2O_3 and its application to fabrication of low-resistance ohmic contacts. *Appl. Phys. Express* **2013**, *6*, 086502. [CrossRef]
84. Oshima, T.; Okuno, T.; Arai, N.; Suzuki, N.; Ohira, S.; Fujita, S. Vertical solar-blind deep-ultraviolet Schottky photodetectors based on β-Ga_2O_3 substrates. *Appl. Phys. Express* **2008**, *1*, 011202. [CrossRef]
85. Wong, M.H.; Sasaki, K.; Kuramata, A.; Yamakoshi, S.; Higashiwaki, M. Field-plated Ga_2O_3 MOSFETs with a breakdown voltage of over 750 V. *IEEE Electron. Device Lett.* **2015**, *37*, 212–215. [CrossRef]
86. Higashiwaki, M.; Kuramata, A.; Murakami, H.; Kumagai, Y. State-of-the-art technologies of gallium oxide power devices. *J. Phys. D Appl. Phys.* **2017**, *50*, 333002. [CrossRef]
87. Bae, J.; Kim, H.Y.; Kim, J. Contacting mechanically exfoliated β-Ga_2O_3 nanobelts for (opto) electronic device applications. *ECS J. Solid State Sci. Technol.* **2016**, *6*, Q3045. [CrossRef]
88. Li, Z.; Liu, Y.; Zhang, A.; Liu, Q.; Shen, C.; Wu, F.; Xu, C.; Chen, M.; Fu, H.; Zhou, C. Quasi-two-dimensional β-Ga_2O_3 field effect transistors with large drain current density and low contact resistance via controlled formation of interfacial oxygen vacancies. *Nano Res.* **2019**, *12*, 143–148. [CrossRef]
89. Spencer, J.A.; Tadjer, M.J.; Jacobs, A.G.; Mastro, M.A.; Lyons, J.L.; Freitas, J.A., Jr.; Gallagher, J.C.; Thieu, Q.T.; Sasaki, K.; Kuramata, A.; et al. Activation of implanted Si, Ge, and Sn donors in high-resistivity halide vapor phase epitaxial β-Ga_2O_3: N with high mobility. *Appl. Phys. Lett* **2022**, *121*, 192102. [CrossRef]
90. Tetzner, K.; Thies, A.; Seyidov, P.; Chou, T.; Rehm, J.; Ostermay, J.; Galazka, Z.; Fiedler, A.; Popp, A.; Würfl, J. Ge-ion implantation and activation in (100) β-Ga_2O_3 for ohmic contact improvement using pulsed rapid thermal annealing. *J. Vac. Sci. Technol. A* **2023**, *41*, 043102. [CrossRef]
91. Tadjer, M.; Lyons, J.; Nepal, N.; Freitas, J.A., Jr.; Koehler, A.; Foster, G. Review-Theory and characterization of doping and defects in β-Ga_2O_3. *ECS J. Solid State Sci. Technol.* **2019**, *8*, Q3187–Q3194. [CrossRef]
92. Nikolskaya, A.; Okulich, E.; Korolev, D.; Stepanov, A.; Nikolichev, D.; Mikhaylov, A.; Tetelbaum, D.; Almaev, A.; Bolzan, C.A.; Buaczik, A., Jr.; et al. Ion implantation in β-Ga_2O_3: Physics and technology. *J. Vac. Sci. Technol. A* **2021**, *39*, 030802. [CrossRef]
93. Huang, H.L.; Chae, C.; Johnson, J.M.; Senckowski, A.; Sharma, S.; Singisetti, U.; Wong, M.; Hwang, J. Atomic scale defect formation and phase transformation in Si implanted β-Ga_2O_3. *APL Mater.* **2023**, *11*, 061113. [CrossRef]
94. Lee, M.H.; Chou, T.S.; Bin Anooz, S.; Galazka, Z.; Popp, A.; Peterson, R. Exploiting the nanostructural anisotropy of β-Ga_2O_3 to demonstrate giant improvement in titanium/gold ohmic contacts. *ACS Nano* **2022**, *16*, 11988–11997. [CrossRef]
95. Zeng, K.; Wallace, J.S.; Heimburger, C.; Sasaki, K.; Kuramata, A.; Masui, T.; Gardella, J.; Singisetti, U. Ga_2O_3 MOSFETs using spin-on-glass source/drain doping technology. *IEEE Electron. Device Lett.* **2017**, *38*, 513–516. [CrossRef]
96. Alema, F.; Peterson, C.; Bhattacharyya, A.; Roy, S.; Krishnamoorthy, S.; Osinsky, A. Low resistance Ohmic contact on epitaxial MOVPE grown β-Ga_2O_3 and β-$(Al_xGa_{1-x})_2O_3$ films. *IEEE Electron. Device Lett.* **2022**, *43*, 1649–1652. [CrossRef]
97. Lee, M.H.; Peterson, R.L. Process and characterization of ohmic contacts for beta-phase gallium oxide. *J. Mater. Res.* **2021**, *36*, 4771–4789. [CrossRef]
98. Kim, H. Control and understanding of metal contacts to β-Ga_2O_3 single crystals: A review. *SN Appl. Sci.* **2022**, *4*, 27. [CrossRef]
99. Oshima, T.; Wakabayashi, R.; Hattori, M.; Hashiguchi, A.; Kawano, N.; Sasaki, K.; Masui, T.; Kuramata, A.; Yamakoshi, S.; Yoshimatsu, K. Formation of indium-tin oxide ohmic contacts for β-Ga_2O_3. *Jpn. J. Appl. Phys.* **2016**, *55*, 1202B7. [CrossRef]
100. Carey, P.H.; Yang, J.; Ren, F.; Hays, D.; Pearton, S.; Kuramata, A.; Kravchenko, I. Improvement of Ohmic contacts on Ga_2O_3 through use of ITO-interlayers. *J. Vac. Sci. Technol. B* **2017**, *35*, 061201. [CrossRef]
101. Carey, P.H.; Yang, J.; Ren, F.; Hays, D.; Pearton, S.; Jang, S.; Kuramata, A.; Kravchenko, I. Ohmic contacts on n-type β-Ga_2O_3 using AZO/Ti/Au. *AIP Adv.* **2017**, *7*, 095313. [CrossRef]
102. Carey IVP, H.; Ren, F.; Hays, D.C.; Gila, B.; Pearton, S.; Jang, S.; Kuramata, A. Band offsets in ITO/Ga_2O_3 heterostructures. *Appl. Surf. Sci.* **2017**, *422*, 179–183. [CrossRef]
103. Carey IVP, H.; Ren, F.; Hays, D.C.; Gila, B.; Pearton, S.; Jang, S.; Kuramata, A. Valence and conduction band offsets in AZO/Ga_2O_3 heterostructures. *Vacuum* **2017**, *141*, 103–108. [CrossRef]
104. Kim, S.; Kim, S.J.; Kim, K.H.; Kim, H.; Kim, T. Improved performance of Ga_2O_3/ITO-based transparent conductive oxide films using hydrogen annealing for near-ultraviolet light-emitting diodes. *Phys. Status Solidi A* **2014**, *211*, 2569–2573. [CrossRef]
105. Sui, Y.; Liang, H.; Chen, Q.; Huo, W.; Du, X.; Mei, Z. Room-temperature ozone sensing capability of IGZO-decorated amorphous Ga_2O_3 films. *ACS Appl. Mater. Interfaces* **2020**, *12*, 8929–8934. [CrossRef]
106. Deng, Y.; Yang, Z.; Xu, T.; Jiang, H.; Ng, K.; Liao, C.; Su, D.; Pei, Y.; Chen, Z.; Wang, G. Band alignment and electrical properties of NiO/β-Ga_2O_3 heterojunctions with different β-Ga_2O_3 orientations. *Appl. Surf. Sci.* **2023**, *622*, 156917. [CrossRef]
107. Ingebrigtsen, M.E.; Vines, L.; Alfieri, G. Bulk β-Ga_2O_3 with (010) and (201) surface orientation: Schottky contacts and point defects. *Mater. Sci. Forum* **2017**, *897*, 755–758. [CrossRef]
108. Yatskiv, R.; Tiagulskyi, S.; Grym, J. Influence of crystallographic orientation on Schottky barrier formation in gallium oxide. *J. Electron. Mater.* **2020**, *49*, 5133–5137. [CrossRef]

109. Wong, M.H.; Nakata, Y.; Kuramata, A.; Yamakoshi, S.; Higashiwaki, M. Enhancement-mode Ga_2O_3 MOSFETs with Si-ion-implanted source and drain. *Appl. Phys. Express* **2017**, *10*, 041101. [CrossRef]
110. Downey, B.P.; Mohney, S.E.; Clark, T.E.; Flemish, J. Reliability of aluminum-bearing ohmic contacts to SiC under high current density. *MicroElectron. Reliab.* **2010**, *50*, 1967–1972. [CrossRef]
111. Liu, L.; Ling, M.; Yang, J.; Xiong, W.; Jia, W.; Wang, G. Efficiency degradation behaviors of current/thermal co-stressed GaN-based blue light emitting diodes with vertical-structure. *J. Appl. Phys.* **2012**, *111*, 093110. [CrossRef]
112. Moens, P.; Banerjee, A.; Constant, A.; Coppens, P.; Caesar, M.; Li, Z.; Vandeweghe, W.; Declercq, F.; Padmanabhan, B.; Jeon, W. Intrinsic reliability assessment of 650V rated AlGaN/GaN based power devices: An industry perspective. *ECS Trans.* **2016**, *72*, 65. [CrossRef]
113. Li, Y.; Ng, G.I.; Arulkumaran, S.; Kumar, C.; Ang, K.; Anand, M.; Wang, H.; Hofstetter, R.; Ye, G. Low-contact-resistance non-gold Ta/Si/Ti/Al/Ni/Ta Ohmic contacts on undoped AlGaN/GaN high-electron-mobility transistors grown on silicon. *Appl. Phys. Express* **2013**, *6*, 116501. [CrossRef]
114. Piazza, M.; Dua, C.; Oualli, M.; Morvan, E.; Carisetti, D.; Wyczisk, F. Degradation of TiAlNiAu as ohmic contact metal for GaN HEMTs. *MicroElectron. Reliab.* **2009**, *49*, 1222–1225. [CrossRef]
115. Jeong, Y.J.; Yang, J.Y.; Lee, C.H.; Park, R.; Lee, G.; Chung, R.; Yoo, G. Fluorine-based plasma treatment for hetero-epitaxial β-Ga_2O_3 MOSFETs. *Appl. Surf. Sci.* **2021**, *558*, 149936. [CrossRef]
116. Zhang, L.Q.; Shi, J.S.; Huang, H.F.; Liu, X.; Zhao, S.; Wang, P.; Zhang, W. Low-temperature Ohmic contact formation in GaN high electron mobility transistors using microwave annealing. *IEEE Electron. Device Lett.* **2015**, *36*, 896–898. [CrossRef]
117. Hou, M.; Xie, G.; Sheng, K. Improved device performance in AlGaN/GaN HEMT by forming ohmic contact with laser annealing. *IEEE Electron. Device Lett.* **2018**, *39*, 1137–1140. [CrossRef]